AIAA 2003–0229

Computational Aerodynamics of the C-130 in Airdrop Configurations
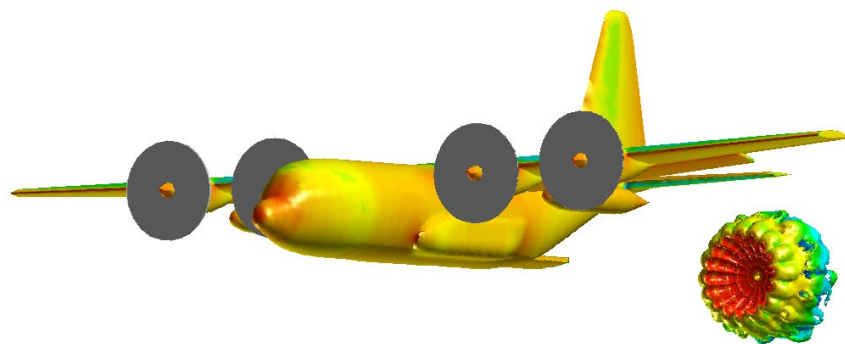
Matthieu Serrano
Ecole Polytechnique, France

Elliot Leigh, William Johnson III, James R. Forsythe, Scott A. Morton
Dept. of Aeronautics, USAF Academy

Kyle D. Squires
MAE Department, Arizona State University, Tempe, AZ

Aerospace Sciences Meeting 2003
6–9 January 2003 / Reno, Nevada

Computational Aerodynamics of the C-130 in Airdrop Configurations

Matthieu Serrano[*]
Ecole Polytechnique, France

Elliot Leigh[†], William Johnson III[‡], James R. Forsythe[§], Scott A. Morton [¶]
Dept. of Aeronautics, USAF Academy

Kyle D. Squires[‖]
MAE Department, Arizona State University, Tempe, AZ

Detached-Eddy Simulation (DES) has been applied to various flight configurations of a complete C-130H airplane. This work is part of a larger research program in which the over-arching aim is to develop the tools for efficient, accurate, and robust calculation of the turbulent flow around a variety of aircraft at flight conditions. The goals of this work are consistent with the longer-term aims of developing DES as a reliable approach for predicting complex flows of engineering interest. The specific objectives of the present investigations have been to use DES to understand the airflows that influence the airdrop of cargo and parachutists. DES combines the efficiency of a Reynolds-averaged turbulence model near the wall with the fidelity of Large Eddy Simulation (LES) in separated regions. Because of the LES treatment in separated regions, it provides more accurate descriptions of the geometry-dependent, three-dimensional unsteady motions comprising regions of massive separation. The current calculations at flight Reynolds numbers were performed using unstructured grids, with cell sizes ranging from 4.5×10^6 to 8×10^6 cells for the entire aircraft. The first configurations considered are the gravity drop and the extraction chute drop without a parachute. To build confidence in the approach and establish a baseline on which subsequent improvements could be made for parachutes, the flow around a T-10 canopy was then computed. DES prediction of the drag coefficient was within 10% of measured values, closer to measurements than other published values for the T-10. The model of a 15 foot extraction chute was then mounted in the turbulent wake of the C-130. The final computation of the C-130 was the personnel drop configuration completing the catalog of all the drop configurations for this aircraft.

Introduction

AIRDROPS are a major component of the ability of a country to project its forces around the world. An important influence that has strong effects on the efficiency and safety of airdrops are the flow fields encountered in various configurations. The flow fields are complex, outside the boundaries amenable to analytic treatment or prediction using simple models that require substantial empirical input. Detailed numerical simulation and modeling comprises an important tool that could be used to provide an improved understanding of the various aspects governing these flows. In the longer term, a numerical simulation methodology could provide a useful tool for assessing the safety of paratroopers and aircrews and aiding future design and developmental testing of new airdrop configurations.

While Computational Fluid Dynamics (CFD) appears to have a strong role for understanding and improving airdrops, the flow fields encountered in airdrop configurations are characterized by regions of massive separation, e.g., as occurs around the paratroop door or in the tailgate region of a C-130 aircraft. Traditionally, such flow fields have been treated using the Reynolds-averaged Navier-Stokes (RANS) equations. While adequate for many attached flows, the performance of RANS methods in separated flows is often poor, leading to large errors in predicting the drag around bluff bodies, for example. The eddies comprising the separated regions of flows with massive separations are unsteady, three-dimensional and usually sensitive to the details of the geometry under consideration. These eddies, arguably, are what defeat RANS models, of any complexity, when applied to flows with massive separation.

Eddy-resolving techniques such as Large-Eddy Simulation (LES) offer strong advantages in prediction of the massively separated flow regions characterizing airdrop configurations. In LES, only the small subgrid scales of motion are modeled. The large eddies, which are responsible for the bulk of momentum transport,

---

[*]Research Assistant
[†]2nd Lieutenant, AIAA Student Member
[‡]2nd Lieutenant, AIAA Student Member
[§]Associate Professor, Senior Member of AIAA
[¶]Associate Professor, Associate Fellow of AIAA
[‖]Professor, Member of AIAA

are resolved directly on the grid. At flight Reynolds numbers, however, LES applied to an entire aircraft is impractical and will remain so for many years (Spalart *et al.* [3]). Detached-Eddy Simulation (DES) was proposed in 1997 by Spalart *et al.* [3] as a computationally feasible approach to provide more accurate predictions of massively separated flows by employing a RANS model in the attached regions of a flow (essentially, the boundary layers prior to separation) along with an LES treatment away from solid surfaces.

Since its inception, DES has been applied to a range of flows, including geometrically simple shapes such as the flow over a cylinder [5] or sphere [6], as well as complex configurations including full aircraft (e.g., see Squires *et al.* [9]). DES predictions of the flow over the F-15E at 65° angle of attack, for example, were within 5% of flight-test data for lift, drag and pitching moment (Forsythe *et al.* [8]). In general, DES has yielded comparable or superior accuracy compared to RANS methods, resolving unsteady, three-dimensional effects in separated regions, while alleviating the Reynolds number limitation that plagues LES. The encouraging performance of the method to date forms one of the primary motivations for the present effort.

In the present contribution, DES is applied to prediction of the flow around the C-130H in various airdrop configurations, including a gravity drop, extraction-chute drop, and personnel drop. The calculations are only the fourth eddy-resolving simulation of a full aircraft performed to date. Predictions of the airdrop configurations are the first of their kind and provide a relatively wide initial knowledge base for examining issues related to aspects such as safety of the jumpmasters while performing door checks and of towed jumpers in static line failures. Because there are no experimental measurements for assessing DES predictions, calculations of the flow around a T-10 canopy were also undertaken in the early phases of this effort. Sahu *et al.* [17] have performed finite-element simulations of the flow around the T-10 canopy for the fluid-structure interaction and finite volume and their solutions offered a baseline for assessing DES predictions in a flow quite relevant to airdrop configurations.

While specifically concerned with airdrop configurations, the computations performed and reported here add to the experience base being developed for accurate and efficient turbulence simulations using DES. The calculations reported in this manuscript challenge not only the underlying turbulence model, but also aspects of the work related to grid generation, performance of large-scale, time-accurate solutions of the Navier-Stokes equations, and issues related to post-processing. Unique features and issues related to the overall computational approach are also reported.

Following is a summary of the theoretical aspects of the turbulence treatment used in the computations. The results of the different configurations will then be presented starting with the gravity drop configuration. The predictions for the extraction chute drop with no extraction chute mounted and the T-10 analysis will be followed by the investigation of the C-130 with a mounted extraction chute. The final investigation will present the C-130 in a personnel drop configuration: with the side doors open and the deflector doors in use. A summary and perspectives gained during the work is provided following results along with recommendations for additional efforts needed to complete this study.

Computational Approach

Spalart-Allmaras Model

The turbulence treatment in the majority of DES work to date is based on the Spalart-Allmaras (SA) one-equation RANS model [2]. In this model, a single partial differential equation is solved for a variable $\widetilde{\nu}$ which is related to the turbulent viscosity. The differential equation is derived by "using empiricism and arguments of dimensional analysis, Galilean invariance and selected dependence on the molecular viscosity."[1] The model includes a wall destruction term that reduces the turbulent viscosity in the log layer and laminar sublayer and trip terms that provides a smooth transition from laminar to turbulent flow. As illustrated by Squires *et al.* [9], the trip terms are important for some of the calculations in order to match conditions of particular experiments. For the current research, the trip terms were turned off and the flow was assumed fully turbulent.

In the S-A RANS model, a transport equation is used to compute a working variable used to form the turbulent eddy viscosity,

$$
\begin{aligned}
\frac{D\widetilde{\nu}}{Dt} &= c_{b1}\widetilde{S}\,\widetilde{\nu} - c_{w1}f_w\left[\frac{\widetilde{\nu}}{d}\right]^2 \\
&+ \frac{1}{\sigma}\left[\nabla\cdot\left((\nu+\widetilde{\nu})\,\nabla\widetilde{\nu}\right) + c_{b2}\left(\nabla\widetilde{\nu}\right)^2\right]
\end{aligned} \tag{1}
$$

where $\widetilde{\nu}$ is the working variable. The eddy viscosity ν_t is obtained from,

$$
\begin{aligned}
\nu_t &= \widetilde{\nu}\,f_{v1} \\
f_{v1} &= \frac{\chi^3}{\chi^3 + c_{v1}^3} \\
\chi &\equiv \frac{\widetilde{\nu}}{\nu}
\end{aligned} \tag{2}
$$

where ν is the molecular viscosity. S is the magnitude of the vorticity, and the modified vorticity is:

$$
\begin{aligned}
\widetilde{S} &\equiv S + \frac{\widetilde{\nu}}{\kappa^2 d^2}f_{v2} \\
f_{v2} &= 1 - \frac{\chi}{1 + \chi f_{v1}}
\end{aligned} \tag{3}
$$

where d is the distance to the closest wall. The wall

destruction function, f_w, is:

$$f_w = g \left[\frac{1 + c_{w3}^6}{g^6 + c_{w3}^6} \right]^{\frac{1}{6}} \qquad (4)$$

$$g = r + c_{w2}(r^6 - r)$$

$$r \equiv \frac{\widetilde{\nu}}{\widetilde{S}\kappa^2 d^2}$$

The closure coefficients are given by:

$$
\begin{array}{lll}
c_{b1} = 0.1355 & \sigma = \frac{2}{3} & c_{b2} = 0.622 \\
\kappa = 0.41 & c_{w1} = \frac{c_{b1}}{\kappa^2} + \frac{(1+c_{b2})}{\sigma} & c_{w2} = 0.3 \\
c_{w3} = 2 & c_{v1} = 7.1 &
\end{array}
$$

$$\qquad (5)$$

Detached-Eddy Simulation

The original DES formulation is based on a modification to the Spalart-Allmaras RANS model [2] such that the model reduces to its RANS formulation near solid surfaces and to a subgrid model away from the wall [3]. DES attempts to take advantage of the usually adequate performance of RANS models in the thin shear layers where these models are calibrated and the power of LES for resolution of geometry-dependent and three-dimensional eddies. The S-A versio of DES is obtained by replacing the distance to the nearest wall, d, by $\widetilde{d}$, where $\widetilde{d}$ is defined as,

$$\widetilde{d} \equiv \min(d, C_{DES}\Delta). \qquad (6)$$

In Eqn. (6), for the computations performed in this project, Δ is the largest distance between the cell center under consideration and the cell center of the neighbors (i.e., those cells sharing a face with the cell in question). In "natural" applications of DES, the wall-parallel grid spacings (e.g., streamwise and spanwise) are at least on the order of the boundary layer thickness and the S-A RANS model is retained throughout the boundary layer, i.e., $\widetilde{d} = d$. Consequently, prediction of boundary layer separation is determined in the "RANS mode" of DES. Away from solid boundaries, the closure is a one-equation model for the sub-grid scale eddy viscosity. When the production and destruction terms of the model are balanced, the length scale $\widetilde{d} = C_{DES}\Delta$ in the LES region yields a Smagorinsky eddy viscosity $\widetilde{\nu} \propto S\Delta^2$. Analogous to classical LES, the role of Δ is to allow the energy cascade down to the grid size; roughly, it makes the pseudo-Kolmogorov length scale, based on the eddy viscosity, proportional to the grid spacing. The additional model constant $C_{DES} = 0.65$ was set through analysis of homogeneous turbulence[4].

Grid considerations

The C-130H and parachute simulations use unstructured grids. These grids are composed of prisms in the boundary layer and tetrahedra outside the boundary layer. The C-130H grids were made using Nasa Langley's Vgridns [10]. The C-130H was only the fourth complete aircraft to be gridded for DES calculations. The first three were the F-16, the F/A-18E and the F-15E. Since then, the X-38 and F-18C have also been successfully run using DES. Only half of the C-130H was actually gridded; the grid was then mirrored about the symmetry plane to allow for the assymetries induced by the propeller disks and resolved turbulence. The calculations were run on the whole aircraft. The various configurations presented in this work and their complexity proved to be challenging for the tetrahedral solver in both Vgridns and Gridgen. In the extraction chute configuration and the personnel drop configuration, the grids were not manageable with the current version of Vgridns (3.3). These configurations served as tests for the beta version of Vgrid 3.5. The T-10 canopy was gridded using the Pointwise Inc. software Gridgen [11]. In this case, the whole canopy was gridded at once.
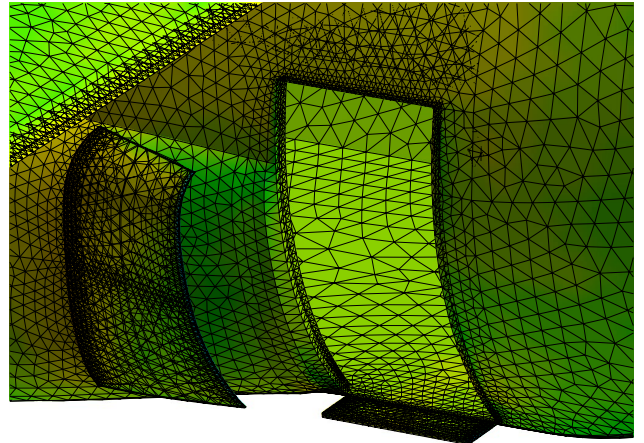

Fig. 1   Detailed view of the surface mesh of the paratroop doors, jump platform and deflector door.

The main issues in the gridding process were encountered at the intersection of a difficult geometric shape with a symmetry plane or in places where too many surfaces converged into a single point. The bottom of the tailgate was one of these areas. Johnson *et al.* [16] solved the problem by adding a small gap between the cargo door and the side of the fuselage to help the tetrahedral solver. By adding a gap, it was easier to compute the surface vectors in that region. The same type of issue was encountered when adding the jump platform in the personnel drop configuration. This issue was solved by reducing slightly the size of the platform. This reduced the singularity at the intersection between the hull, the door, and the jump platform helping the tetrahedral solver in computing the surface vectors. When the deflector door was added on the C-130, the door was very close to the aircraft but included a small gap. During the viscous grid generation process, the viscous grid from the door would grow into the viscous grid from the aircraft

and cause the grid generator to fail. This problem was solved by using Vgrid 3.5, which has an improved algorithm for the generation of viscous grids.

The parachutes were also problematic to grid. In both Vgrid and Gridgen, it was necessary to add a small finite thickness to the parachute; both grid generators refusing to grow a viscous grid and wrap it around the edges of a surface. This small thickness was challenging for both tetrahedral solvers and required special care. Moreover, for the extraction chute configuration, we had to grid only half of the extraction chute. In this case, the symmetry plane cut the parachute in two. When growing the volume grid, at the intersection of the symmetry plane and this thickness, the grid would grow through the symmetry plane. Originally, this intersection was between two gores. This created a very narrow region between the parachute and the symmetry plane. The parachute was then rotated to have the intersection occur in the middle of the gore, improving the angle between the parachute and the symmetry plane. Even with this modification, the grid generator was unable to generate the grid with version 3.3, requiring the new version of Vgrid.

Flow solver

The compressible Navier-Stokes solver forming the backbone of this study is Cobalt, a commercial version of $Cobalt_{60}$ — a compressible solver developed at the Air Force Research Laboratory in support of the Common High Performance Software Support Initiative (CHSSI). The relevant improvements available in the commercial version and central to the success of the current project are faster per-iteration times, ability to calculate time-averages and turbulence statistics, an improved spatial operator, and improved temporal integration. Strang et al.[7] validated the code on a number of problems, including the Spalart-Allmaras model (which forms the core of the DES model). Tomaro et al.[12] converted $Cobalt_{60}$ from explicit to implicit time integration, enabling CFL numbers as high as one million. Grismer et al.[13] then parallelized the code, yielding a linear speedup on as many as 1024 processors. Parallel METIS domain decomposition library of Karypis et al.[14] [15] is incorporated in Cobalt. ParMetis divides the grid into nearly equally sized zones that are then distributed one per processor.

Cobalt is a second-order hybrid unstructured parallel solver, with second-order accuracy in space and time. Cobalt has been used in many of the calculations done by Squires et al.[9] and has proved to give accurate results on full aircraft and massively seperated flows.

The C-130H performs airdrops at speeds between 130 and 140KIAS and at altitudes ranging from 500ft to 25,000ft. The Reynolds number based on the chord used in these calculations will therefore range from 8.6

million to 17.8 million. The grids were designed to provide an average surface normal spacing in wall units y^+ less than 1 for the first cell off the wall for the whole aircraft. The average y^+ for the grids developed for this work was 0.2.

The C-130H has four engines. These propellers are modeled in Cobalt by using an actuator disk boundary condition. The propellers are set to all turn in the same direction, as on the actual aircraft. They were set to turn at 1020 RPM and deliver 3000lb of thrust each. The peak loading position of the blades was set at 90% of the propeller radius, with a linear load distribution assumed.

Validation Cases

C-130 in gravity drop configuration

An initial study of the C-130 with the tailgate (rear lower door) down was initiated by Johnson et al. [16]. These calculations were performed at a low Reynolds number in order to match experimental measurements. Starting from these encouraging results, the grid has been modified to make it even more faithful to the actual aircraft and the calculations were run at flight Reynolds number.

In a gravity drop configuration, the C-130 has its tailgate down and is at an angle of attack between 8° and 10°. The containers then roll out of the hull once they are released. This angle is achieved by setting the flaps according to the payload weight. The computations were performed at 8° angle of attack with flap settings at 35%.

In both investigations presented here, the C-130 will be set at 140KIAS (M = 0.21) at 1000ft MSL. The corresponding Reynolds number is 1,488,000/ft. The grid is comprised of 4.5 million cells with 14 layers recombined in prisms in the boundary layer.

Steady investigation

Elliot Leigh and William Johnson III in their final CFD project at the USAF Academy performed a RANS study of the C-130 in gravity drop configuration. In association with this study, the grid was modified from the original C-130 grid [16]. The major modifications were the modeling of the exact dimensions and geometry of the back door and the addition of the fuel tanks. The cavity inside the airplane was also enlarged.

This study was performed using the Spalart Allmaras RANS turbulence model and showed that the vortices at the aft of the airplane develop at the base of the ramp. These vortices create a region with high vertical velocity (figure 2). The vertical velocity peaks at half of the free stream velocity. Johnson et al.[16] had already identified this as the reason why static line paratroop jumps are not routinely made out of the aft cargo doors. Indeed, if the static line should fail, the paratroop would be dragged through that region of
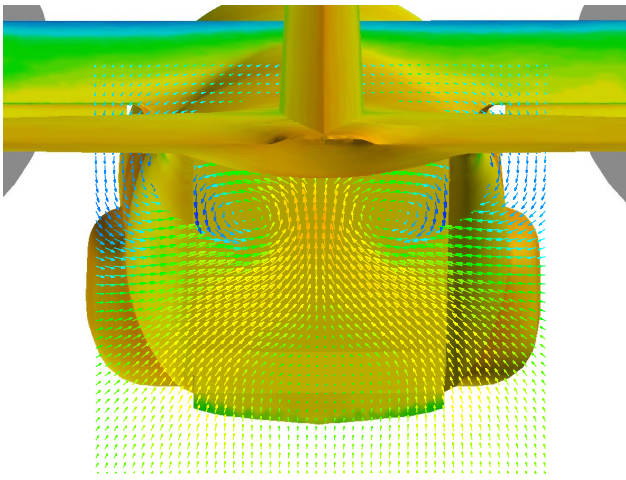
Fig. 2   Velocity vectors colored by W-velocity. Visualization of the two main vortices.

high vertical velocity and risk striking the top of the hull.

Unsteady investigation

The DES study resolved more unsteadiness in the flow in the tailgate region (figure 3).
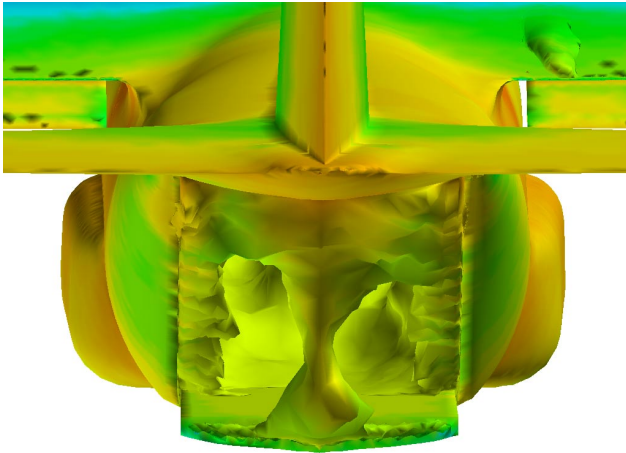

Fig. 3   Isosurface of U-velocity = 0 − Separation bubble in the tailgate region.

The cavity in the back of the aircraft is relatively free of instabilities. The instantaneous flow is not completely symmetric and some smaller turbulent structures do exist, demonstrating that the DES calculations were not in RANS mode in that region. Grid refinement is recommended in order to rule out the possibility that the grid coarseness is damping the unsteadiness. Nevertheless, the vortices shown in the steady calculations seem to provide a stabilizing that may tend to dampen the strength of the smaller structures.

Conclusion

In the region investigated, the RANS calculations have shown the most salient flow features - the strong vortex pair causing the induced upward velocity. The

DES calculations showed these structures as well, and resolved some unsteadiness in the cargo region. In this flow, the RANS calculations gave most of the qualitative results necessary. Unfortunately, the quantitative accuracy of the two methods for this flow is unkown at this point due to a lack of unsteady experimental or flight test data. Further work would include grid refinement in order to see sensitive the cavity and the near wake are to grid refinement. It is important to note that these simulations provide useful information on the regions of interest that need to be focused on during future experiments which include wind tunnel and flight tests.

Flow around a rigid canopy

Before mounting the extraction chute to the C-130 grid, the method was validated by studying the flow around a rigid, non-porous canopy in a steady descent. The results using DES are compared to both experimental data and other computational flows done by Sahu *et al.*[17]. These computations are made on a T-10 canopy, the standard US Army chute, at a Reynolds number of 4 million based on the nominal diameter corresponding to a steady descent of a 300lb load in a 18 ft/s descent. This parachute has a nominal diameter of 35ft.

Canopy geometry

The inflated geometry was provided by Sahu *et al.* This shape had been calculated by a finite element fluid-structure interaction (FSI) program. The calculations were made on the same geometry but the grid was regrown using Gridgen. This grid (figures 4 and 5) is composed of 4.25 million cells including 2.2 million prisms in the boundary layer.
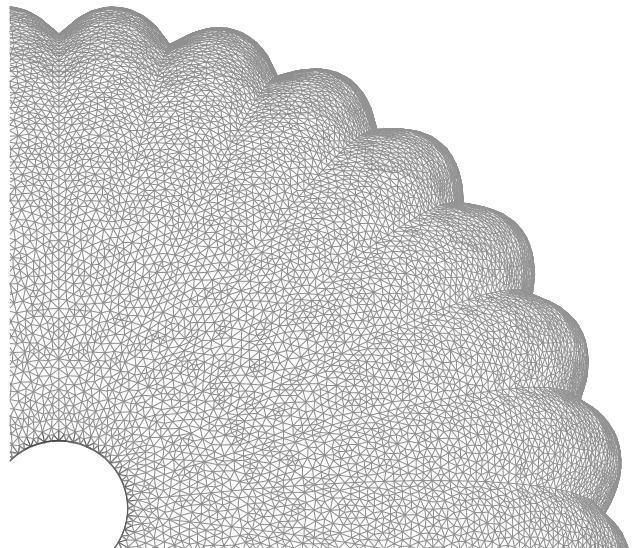

Fig. 4   Detailed view of the surface mesh of the T-10 parachute.

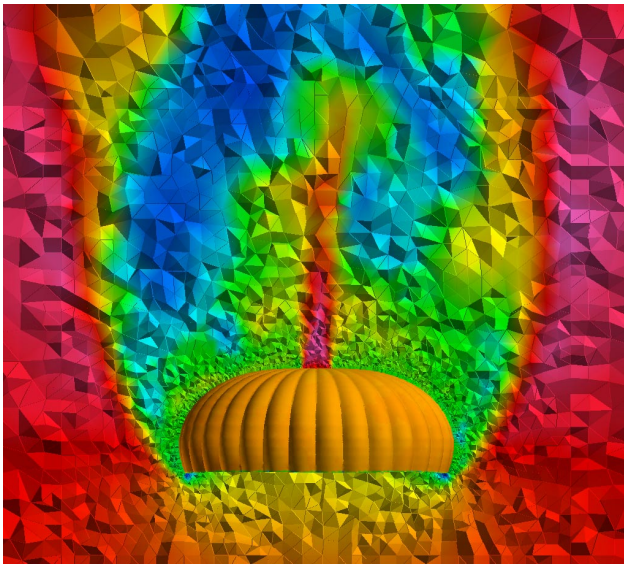The T-10 is a flat extended skirt parachute [18]. In this case, the skirt is a 10% extension. For this

Fig. 5 Grid of the T-10 parachute colored by U-velocity.

Fig. 6 Convergence of the T-10 calculations (forces in pounds). Fx represents the drag on the chute, while Fy and Fz represent side forces.

shape, the ratio between the inflated diameter and the nominal diameter varies from 0.66 to 0.70. The associated drag coefficients based on the inflated diameter vary from 0.78 to 0.87. The nominal diameter D_0 is calculated knowing the total surface of a parachute, including the main hole, S_0 by $D_0 = \sqrt{(4 * S_0/\pi)}$. Unfortunately, Sahu *et al.* did not take into account the extended skirt in the calculation of the surface and therefore oversized the parachute. Once this correction was made, the inflated shape had a diameter of 23.1ft. The corresponding drag coefficient on the actual T-10 canopy was 0.78.

Sahu *et al.*[17] used an unstructured finite volume solver to compute laminar, turbulent one-equation and turbulent two-equation models resulting in C_D of 0.78, 0.77, and 0.75 respectively. Their finite-element Smagorinsky code predicted a C_D of 0.89. These results need to be rescaled by taking into account the surface of the extended skirt. The recomputed C_D are 0.57, 0.56, 0.55 and 0.66 for their finite element code.

Nevertheless, this mesh has provided some useful information on inflated shapes. For instance, the FSI program has calculated an extension for the length scales of 3%. The radial shape of the gores was spline fitted to get a smoother surface. This showed that the nondimensional radial shape of the gore is almost uniform over the whole parachute. Moreover, the ratio between the height of the parachute and the nominal radius is 0.40. These features have been used to create a model for the inflated shapes of the extraction chutes.

Results

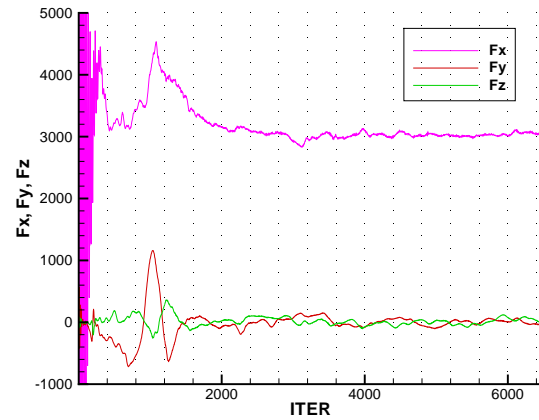The DES computations were run for 6500 iterations which corresponds to 130 nondimensional time units (made nondimensional by the parachute diameter and the freestream velocity). The results were free of inital transients after 2000 iterations (Figure 6) and gave an average drag coefficient of 0.70 when averaged over the final 4000 iterations. The side forces were very small compared to the drag and the resultant force oscillates and presents a peak angle with the freestream velocity of 2 degrees. The average angle of oscillation for this type of canopy is typically between 10 and 20 degrees. The amplitude of these oscillations are most likely due to a dynamic process and would therefore need a more elaborate code to predict. It is recommended that further study include grid refinement and the use of an aeroelastic code. This type of code could predict the "breathing" of the parachute and also the amplitude of the natural oscillations of the canopy.
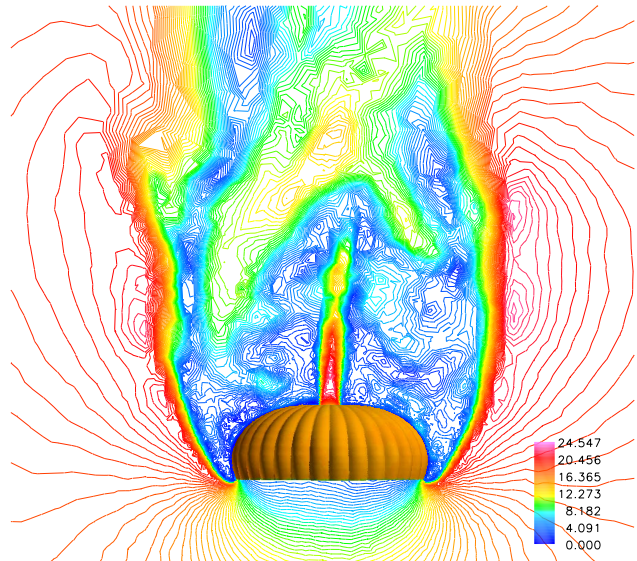

Fig. 7 Computed velocity magnitude contours on the T-10 chute.

In the current computations, the flow detaches from the bottom of the skirt (figures 7 and 8). The shear

layer then creates a cylinder with a radius of approximately 1.5 times the inflated radius of the chute. The cylinder enclosing the separation bubble has a height of three times the height of the parachute or 2/3 of the nominal diameter of the chute. Inside this region a fine grid is required to resolve the turbulent structures in LES mode.
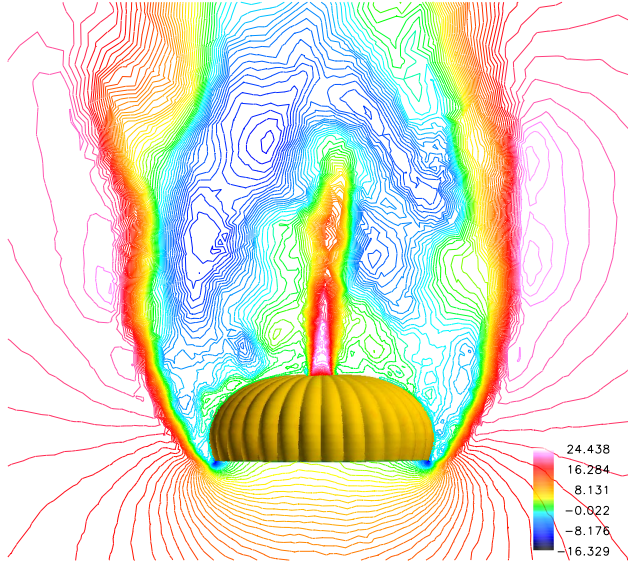

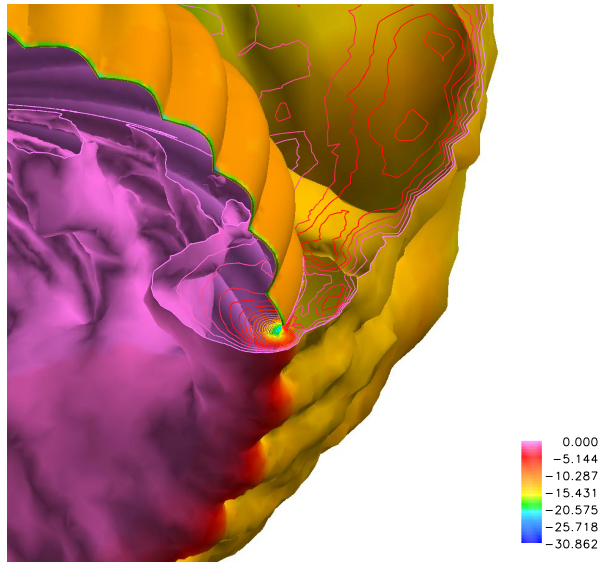**Fig. 8   Computed U-velocity magnitude contours on the T-10 chute.**

Fig. 9   Iso-surface and contours of negative U-velocities.

This computation shows that a grid around a canopy should be fine in the cylinder described above. In this respect, the grid on which these calculations were made is an efficient grid, since it emplyed a fine grid in this region, and rapidly coarsened outside of the region. Nevertheless, grid refinement, as always in computational studies would provide a better understanding of the quality of the current grid.

	C_D	
Actual T-10 Canopy	0.78	
Sahu *et al.*[17]	Original	Corrected
laminar	0.78	0.57
turbulent one-equation	0.77	0.56
turbulent two-equation	0.75	0.55
Smagorinsky finite element	0.89	0.66
DES	0.70	

Table 1   Comparison of computed drag coefficients of the T-10 canopy

The shear layer rolls up and it is these vortices which create the side forces. A finer grid near the bottom of the chute could refine the position of the roll-up and eventually give more accurate side forces. Nevertheless, figure 9 shows that close to the bottom edge of the chute, there is a region with high velocity pointed upstream. The value of this velocity is roughly 1.5 times the free stream velocity. This shows that strong local forces are applied to the bottom of the canopy and that if this parachute was not rigid, a breathing motion would start in that region. The temporal variations of this region show that the time scale for the flow inside the canopy is much slower than the one associated with the shear layer roll-up.

Conclusion

This brief study of the T-10 parachute showed that flows around parachutes is a natural application of DES. Predictions of the drag coefficient (Tab. 1) were under-estimated by 10%. Although no grid refinement study was performed for this study, the experience learned from Morton *et al.*[20] gives confidence in these results, since a similar grid strategy was employed. Nevertheless, a more accurate prediction of the flow would require eliminiation of the rigid non-porous model of the canopy. For round parachutes, the dynamic effects of breathing and oscillations should be considered. But, the current results give enough confidence in the rigid method that mounting an extraction chute on the C-130 is useful.

Investigation of different configurations

The validation of our method using the prior numerical results and wind tunnel tests for the C-130 in gravity drop configuration and the results concerning the rigid canopy simulations motivated the study of all the different airdrop configurations. The focus of this project was to study the feasability of this type of investigation in a short time in order to be a valuable help for the definition of the experiments (both wind tunnel and flight tests) that will be done in the near future.

The configurations left to be investigated were the extraction chute drop and the personnel drop configurations. In light of the aim of this study, we have

set the flaps for all the simulations to be the same as for the gravity drop. Therefore, in all the grids considered, the flaps are set at 35%. Although in actual airdrops, the flap setting would be between 50% and 60%, the lack of experimental data to compare to made this simplification reasonable.

The extraction chute drop uses the same flight configuration as above with the lower aft cargo door down and the upper aft cargo door up. In this case, the aircraft is flying level. A parachute is then released into the flowfield and the resulting tension in the lines extracts the cargo out of the hull. The computations are first made using the previous grid at 0° angle of attack with no extraction chute. An extraction chute was then added to the grid.

The final configuration studied is the C-130H with the side paratroop doors open. A jump platform is installed and the deflector doors are in use. In order to accurately predict this flow, a significant amount of cells were needed in the region around the deflector doors and the paratroop doors. This led to the largest grid in this study having nearly 8 million cells.

Extraction chute geometry

The geometry for the extraction chute was developed using the knowledge learned from the geometry of the T-10 and empirical data. The flat shape for this ringslot parachute is known; therefore, the size of the rings and of the slots were known. The number of gores is also known. The projected shape is a circle; the ratio between the inflated diameter and the nominal diameter is 0.66 [18]. The profile for the parachute was arbitrarily chosen as elliptical. This shape gives the required "flat" aspect to the profile near the main vent and near the tip of the parachute. In order to conserve the surface of the parachute, the ratio between the inflated height and the nominal radius was set to 0.60. A nondimensional profile was chosen for the gores. This profile was then scaled along the gore in order to keep the length within the 3% value observed on the T-10 canopy. The slots were also widened in the extraction model. This can be seen on the actual extraction chutes and comes from the way the rings are actually inflated.

The geometry described above was used to create the inflated shapes of all the extraction chutes currently used by the military. These are the 15ft, 22ft and 28ft extraction chutes.

The geometry is purely empirical and does not exactly represent the actual extraction chutes. Nevertheless, when comparing the model to pictures of the actual extraction chutes, the model appears very close. Moreover, it appears that the drag coefficient and therefore the efficiency of a parachute depends more on the projected area than on a specific inflated shape (if the differences are not too extreme). In further studies, the inflated shape could be refined and

eventually be calculated using an FSI program. The major improvement would concern the elliptical profile. A more elaborate profile could make the chute much flatter near the main vent and bring the ratio between the inflated height and the nominal radius closer to 0.40.

Greater accuracy could be obtained with the use of an aeroelastic code which could predict both the inflated shape and make the parachute non rigid and non static.

Results

C-130 in extraction chute drop configuration

The calculations with no extraction chute were run for 3000 iterations which corresponds to 60 nondimensional time units. The results were free from the initial transients after 2000 iterations.

The vortices observed in the gravity drop configuration were still present and are as strong as in the previous case. The separation in the tailgate region was also very similar to the one in the gravity drop configuration. This separation bubble (figure 3) creates a region in the middle of the ramp well known to C-130 crews to be free of buffeting.
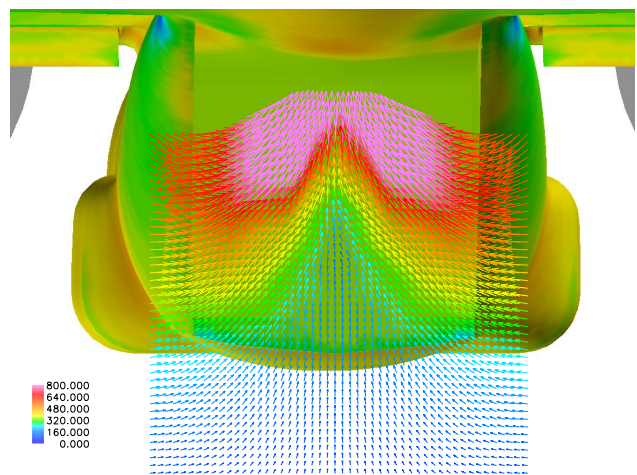

Fig. 10   Velocity vectors 16ft aft of the ramp colored by W-velocity.

One of the purposes of this calculation was the investigation of the flow in which the extraction chute was to be mounted. The position of the extraction chute can vary from 16ft to 49ft aft of the cargo ramp. This flow shows that if the extraction chute is less than 30ft aft of the tailgate, the top of the canopy will be caught in a region where the upward velocity will be high (1/3 the freestream velocity). This is especially true 16ft aft. This is a region where the rigid static canopy assumption will not accurately predict the actual flow. In this case, accurate predictions would require an aeroelastic code. Nevertheless, with the extraction chute placed at a distance over 30ft aft of the ramp, the flow is smooth (the velocities present a maximum angle with the freestream velocity of 5°)

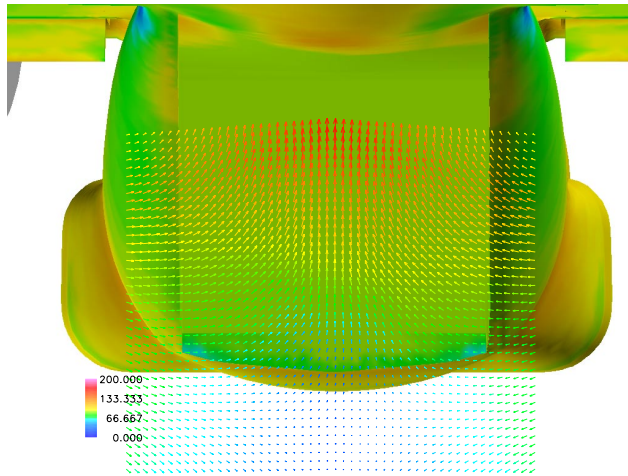and the static rigid model should be a fair first assessment.

Fig. 11 Velocity vectors 49ft aft of the ramp colored by W-velocity.

Conclusion

This calculation shows that using a rigid static model for the extraction chute is a fair first estimate under the condition that the chute is farther than 30ft aft of the tailgate. Using this type of model closer to the aircraft would show a lot of interaction between the turbulent wake of the aircraft and the extraction chute and the results should then be considered with care.

The military are currently investigating the use of extraction lines of 80ft for use on the C-130J-30, the stretched version of the C-130J. This version is 18ft longer than the C-130H and C-130J. In an effort to unify the equipment on the different versions of the C-130, there is an investigation to see if the 80ft extraction line could be used on the short versions of the C-130. According to these calculations, the use of this extraction line would be an improvement since the extraction chute would never be closer than 36ft of the cargo ramp. The flow in which the parachute would inflate would than be less turbulent.

C-130 with mounted extraction chute

After studying the flow around a standard chute, an extraction chute is mounted in the flow aft of the C-130H. This chute is a ringslot [19] parachute and uses a 60ft extraction line. The position of this chute is therefore between 16 and 49ft aft of the cargo ramp. These computations are a first step toward predicting the most efficient position and the possible interactions with the downstream vortices. These computations could also help predict the proper sizing of the extraction chutes.

Due to the issues related to griding such a complex geometry, only one configuration was run. A 15 feet extraction chute was mounted 49 feet aft of the cargo ramp. This configuration was run on a grid with 7.2 million cells. As was learned in the the study of the T-10 canopy , the grid was made fine in a cylinder behind the extraction chute (figure 12). An automatic method for placing and griding the extraction chute was made. This was coupled with the method creating the inflated shapes for the extraction chute. Therefore, if no new griding issues are discovered, creating a new grid with another extraction chute at any position in the wake of the C-130 can be made in less than a day. The only limitation is currently that only half of the C-130 is gridded and then mirrored. This means that the extraction chute will need to be mirrored and that the center of the chute needs to be on the symmetry plane.
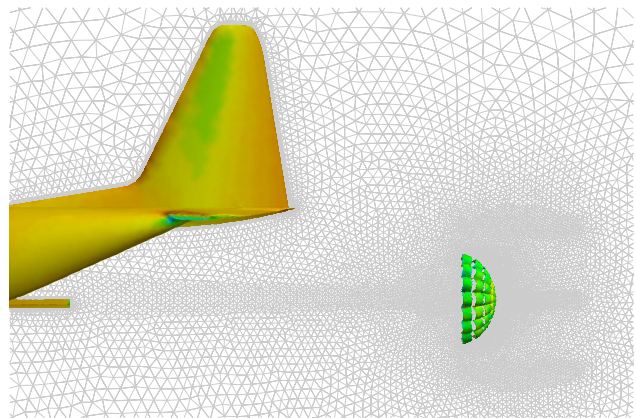

Fig. 12 Grid of the C-130H with the mounted extraction chute colored by pressure.

In this configuration, the calculations were run for 3500 iterations and the results are well converged for both the aircraft and the extraction chute. The lift is consistent with the calculations for the C-130 in an extraction chute drop configuration but without any extraction chute. The difference in the drag is probably due to the interference with the extraction chute. The extraction chute has a drag of 5300lb, giving a drag coefficient of 0.47. The drag coefficient for an actual ringslot extraction chute in a steady descent with this inflated shape is 0.56 [18]. The difference between the ringslot extraction chute drag alone and the chute in teh wake of the C-130 may be due to the interaction between the C-130 wake and the extraction chute (see figure 16), due to modeling erros, or both. Figure 13 depict the relationship between the chute and the C-130 and also shows the shear layer separation aft of the chute.

The wake of the extraction chute is similar to that of the T-10 canopy. There are nevertheless some differences. The wake of the extraction chute is much longer than that of the T-10 canopy. More precisely the fine structures in the wake of the chute occupy a cylinder with a radius slightly smaller than that of the T-10 but with the same height. Over this cylinder, another cylinder of the same size contains much bigger turbulent structure which do not require so fine a grid.

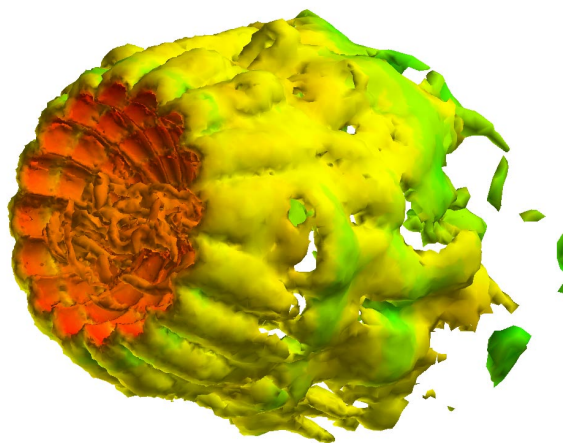**Fig. 13   Iso-surface of vorticity on a 15ft extraction chute behind a C-130H.**

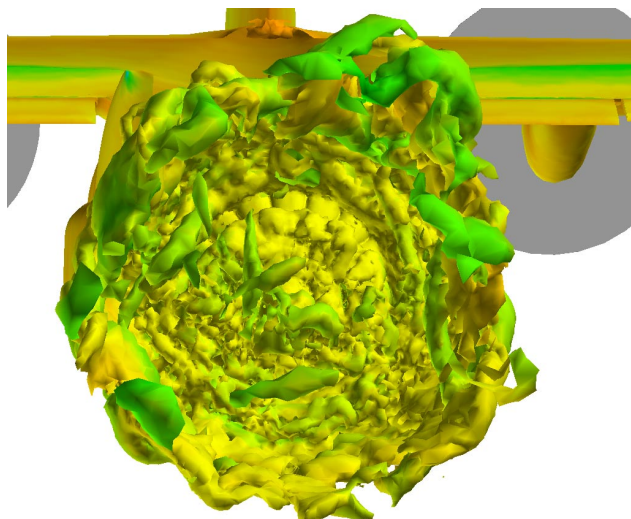**Fig. 14   Detailed view of the iso-surface of vorticity on a 15ft extraction chute.**

Fig. 15   Detailed view of the iso-surface of vorticity on a 15ft extraction chute.

Nevertheless, unlike the T-10 canopy, the shear layer does not appear to roll up. The side forces for this extraction chute are also very small as for the T-10. The ringslot parachute had average angles of oscillations of the resultant force of less than 5°.

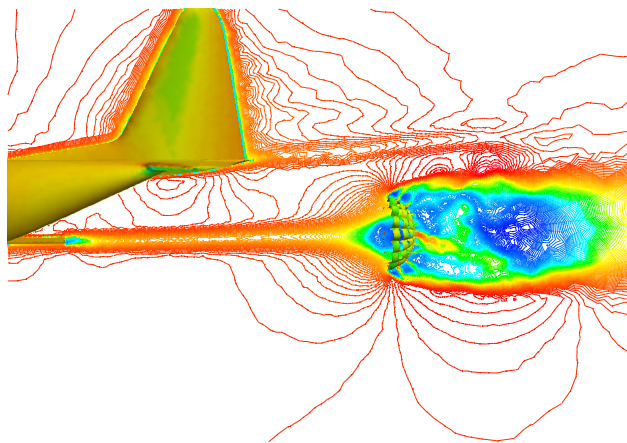On figures 16 and 17, the effect of the slots can be seen as the air flow through (geometric porosity).

Fig. 16   Computed U-velocity magnitude contours on the 15ft extraction chute.
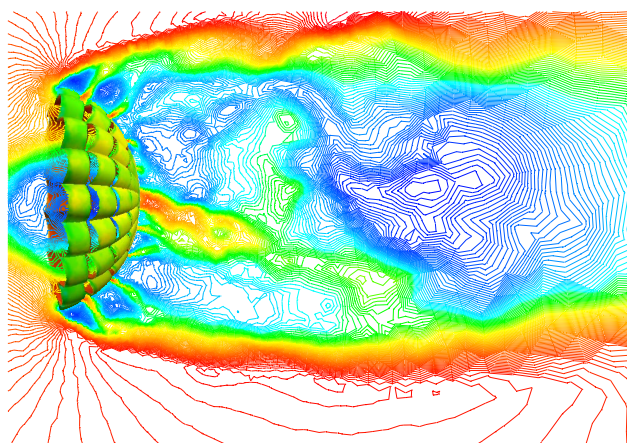

Fig. 17   Detailed view of the computed U-velocity magnitude contours on the 15ft extraction chute.

Conclusion

Many aspects of this complex geometry requires further work in order to determine more accurate results. Future work could include the extraction chute alone in order to quantify the drop of drag coefficient due to the wake of the aircraft. Determining the drag of the extraction chute in the wake can also help sizing the extraction chute and the elements holding the main parachutes of the cargo crate. These parachutes should not be opened before the cargo has cleared the cargo bay or else the aircraft could be severely crippled. It should be noted that using these calculations for such an application, the opening shock should also be considered. Modelling the opening shock would require a fluid structure interaction program.

On at least one of the various configurations that can be investigated in future work with different extraction chutes in different positions, a grid refinement study should be made in order to assess the accuracy of these results. Moreover, an analysis of the extraction chute by itself would be useful to estimate the impact of the C-130 on the efficiency of the extraction chutes. As was previously noted on the T-10 canopy, the use of an aeroelastic code should be used to more accurately predict the flow around a parachute, especially in the region closer than 30ft.

C-130 with paratroop doors opened

The calculations were run for 3000 iterations which was barely enough to get past the intial startup transients.

Fig. 18   Iso-surface of vorticity on the C-130H in personnel drop configuration. Preliminary run without the deflector door and jump platform.

A preliminary run was made with only the doors open. The deflector doors and jump platforms had not yet been added (figure 18). These results therefore do not represent the actual C-130 in personnel drop configuration. But the results allow us to visualize the effect of the deflector doors and the jump platforms. This preliminary run had a coarse grid on the wings exhibiting significant separation over the wings. All other grids were refined which eliminated the flow seperation at 0° angle of attack.

The deflector door has a very significant effect on the flow in the area of the paratroop doors. In the preliminary run without the deflector door, a separation bubble was created on the top of the door but the flow does not detach in a significant manner on the bottom part of the door. When the deflector door is not in place, the flow outside of the paratroop doors is not detached and is therefore a region with high velocity. In this case, door checks and actual jumps would be done in very dynamic air flows. With the deflector door in use, the flow is significantly separated all over the paratroop door providing an environment with much lower velocity in the vicinity of the door.
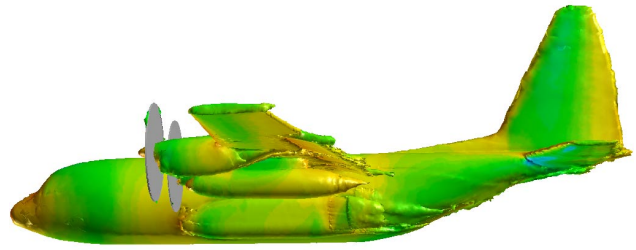

Fig. 19   Iso-surface of vorticity colored by pressure on the C-130H in personnel drop configuration.

The safety during door checks was one of the issues which motivated this investigation. The use of the deflector door creates a region around the paratroop doors which makes the area safer. The deflector doors should be used on the C-130 when the paratroop doors are open. These two calculations are a good demonstration of the use of such a device, and show the usefulness of a computational tool for the design of these devices.

The flow in the wake of the aircraft is similar to that of the extraction chute configuration. The two main vortices present in both the gravity drop and the extraction chute configuration are still present but have significantly less strength.

Conclusion

This investigation of the flow around the open paratroop doors of the C-130H shows the utility and the effectiveness of the deflector doors. This investigation was also able to predict the dynamics of the flow in that area and therefore the safety of that region. Although calculations should be done on the C-130J to confirm this, these calculations allow us to predict that the aircraft presents a smoother flow aft of the paratroop doors and therefore be safer in the event of a towed jumper. As always, grid refinement should be done on this configuration to display more turbulent structure and to confirm these results.

Concluding remarks

DES has been used to study the flow around the C-130H in different airdrop configurations. These results allow us to have a more precise understanding of the near wake behind the aircraft and the airflow around the opened doors. This study has shown that DES allows the engineer to have a view of the aircraft in numerous flight configurations. All griding work and computations took place over a three month time frame, showing that the tools used could be applied for engineering predictions.

In these computations, creating grids for these complex geometries proved to be a real challenge. This area is where the most progress needs to be made to make CFD a more accessible tool. The various grid generators have different flaws and assets. Vgrid uses nodal and linear sources to define the cell sizes when Gridgen defines a uniform spacing directly on the surface. The latter makes gridding surfaces such as wings much easier but a linear source can be very useful to refine the grid in the core of a vortex. Future grid generators should allow the user to use both methods. This would make it much easier to grid a whole aircraft.

As the computational cost of these calculations become more and more accessible, the geometries investigated will become more and more complex. The grid generation algorithms should become more robust in order to avoid the issues encountered in this study. The step from the CAD files to the grid should become faster and easier and in the end almost automatic. Adaptive mesh refinement will also be a significant improvement and would increase the usefulness of the cells present in the grid.

Numerical accuracy of the flow solver is also an issue and an area where progress could still be made. The unstructured solver used was second order accurate, as is typical for unstructured codes. Implementation of a higher order method, or a lower dissipation algorithm could enhance the current calculations. However, the levels of unsteadiness resolved for the current coarse grids is encouraging. Also, a low order of accuracy can nevertheless be compensated by a higher number of cells, motivating the use of adaptive mesh refinement.

This study has shown the efficiency of DES and the *Cobalt* code to investigate unsteady flows around full aircraft. This investigation gave a thorough view of the different airdrop configurations of the C-130H. Although future work is still needed to complete this study, it has shown that DES combined with unstructured grids allows CFD to be useful as an engineering tool for analyzing separated flows over aircraft.

Acknowledgments

References

[1] Spalart, P. R., "Strategies for Turbulence Modeling and Simulations," 4th Int. Symp. Eng. Turb. Modelling and Measurements, Corsica, May 24-26, 1999.

[2] Spalart, P.R. and Allmaras, S.R., 1994, "A One-Equation Turbulence Model for Aerodynamic Flows," *La Recherche Aerospatiale* **1**, pp. 5-21.

[3] Spalart, P. R. , Jou W-H. , Strelets M. , and Allmaras, S. R., "Comments on the Feasibility of LES for Wings, and on a Hybrid RANS/LES Approach," *Advances in DNS/LES, 1st AFOSR Int. Conf. on DNS/LES*, Aug 4-8, 1997, Greyden Press, Columbus Oh.

[4] Shur, M., Spalart, P. R., Strelets, M., and Travin, A, "Detached-Eddy Simulation of an Airfoil at High Angle of Attack, 4th Int. Symp. Eng. Turb. Modelling and Measurements, Corsica, May 24-26, 1999.

[5] Travin, A., Shur, M., Strelets, M., and Spalart, P.R., 2000, "Detached-Eddy Simulation Past a Circular Cylinder," *Int. J. Flow, Turbulence and Combustion*, 63(1-4), pp. 293–313.

[6] Constantinescu, G.S., and Squires, K.D., 2000, "LES and DES Investigations of Turbulent Flow over a Sphere," AIAA Paper 2000-0540.

[7] Strang, W. Z., Tomaro, R. F, Grismer, M. J., "The Defining Methods of Cobalt$_{60}$: a Parallel, Implicit, Unstructured Euler/Navier-Stokes Flow Solver," *AIAA 99-0786,* January 1999.

[8] Forsythe J.R., Squires K.D., Wurtzler K.E. and Spalart P.R., "Detached-Eddy Simulation of fighter aircraft at high alpha", *AIAA Paper 2002-0591*, 2002.

[9] K.D. Squires, J.R. Forsythe, S.A. Morton, W.Z. Strang, K.E. Wurtzler, R.F. Tomaro, M.J. Grismer and P.R. Spalart, "Progress on Detached-Eddy Simulation of massively separated flows", *AIAA Paper 2002-1021*, 2002.

[10] Pirzadeh, S., "Three-dimensional Unstructured Viscous Grids by the Advancing Layers Method," *AIAA Journal*, 1996, **34**, pp. 43-49.

[11] Steinbrenner, J., Wyman, N., Chawner, J., "Development and Implementation of Gridgen's Hyperbolic PDE and Extrusion Methods," *AIAA 00-0679*, January 2000.

[12] Tomaro, R.F., Strang, W. Z., and Sankar, L. N., "An Implicit Algorithm for Solving Time Dependent Flows on Unstructured Grids," *AIAA 97-0333*, January 1997.

[13] Grismer, M. J., Strang, W. Z., Tomaro, R. F. and Witzemman, F. C., "Cobalt: A Parallel, Implicit, Unstructured Euler/Navier-Stokes Solver," *Advances in Engineering Software*, Vol. 29, No. 3-6, pp. 365—373, 1998.

[14] Karypis, G., and Kumar, V., *METIS: Unstructured Graph Partitioning and Sparse Matrix Ordering System Version 2.0.* University of Minnesota, Department of Computer Science, Minneapolis, MN 55455, July 1997.

[15] Karypis, G., Schloegel, K., and Kumar, V, *ParMETIS: Parallel Graph Partitioning and Sparse Matrix Ordering Library Version 1.0.* University of Minnesota, Department of Computer Science, Minneapolis, MN 55455, July 1997.

[16] Johnson, W. III, Trickey, C., Forsythe, J. R., Albertson, J., Leigh, E., 2002, "Experimental and Computational Investigation of the Flow behind a C-130 with Tailgate Down," *AIAA 02-0713*.

[17] Sahu, J., Edge, H., Heavey, K., Chakravarthy, S., Stein, K., and Benney, R., "Comparison of Numerical Flow Field Predictions for Army Airdrop Systems," *AIAA 99-1715*, Proceedings of the 15th CEAS/AIAA Aerodynamic Decelerator Systems Technology Conference and Seminar, Toulouse, France (1999).

[18] Knacke, T. W., "Parachute Recovery Systems Design Manual" Santa Barbara, CA: Para Publishing, 1992.

[19] Ewing, E.G., Bixby, H. W., Knacke, T. W., "Recovery Systems Design Manual" U.S. Air Force Flight Dynamics Laboratory, Technical Report AFFDL-TR-78-151, December 1978.

[20] S.A. Morton, J.R. Forsythe, K.D. Squires and K.E. Wurtzler, "Assessment of unstructured grids for Detached-Eddy Simulation of high Reynolds number separated flows", *Proceedings of the Eighth International Conference on Numerical Grid Generation in Computational Field Simulations*, 2002.